SEMI-LAGRANGIAN HIGH-ORDER 3D INTERPOLATION: SURVEY ON A FINITE ELEMENT Z-TYPE OPERATOR

Gustavo Charles Peixoto de Oliveira, tavolesliv@gmail.com

University of the State of Rio de Janeiro, Faculty of Engineering, R. Fonseca Teles, 121, São Cristóvão, Rio de Janeiro, RJ, Brazil, 20940-903

Norberto Mangiavacchi, norberto@uerj.br

University of the State of Rio de Janeiro, Faculty of Engineering, R. Fonseca Teles, 121, São Cristóvão, Rio de Janeiro, RJ, Brazil, 20940-903

José Pontes, jopontes@metalmat.ufrj.br

Federal University of Rio de Janeiro, Metallurgy and Materials Engineering Department, Rio de Janeiro, RJ, Brazil, PO Box 68505, 21941-972

Abstract. *Discrete models using Semi-Lagrangian advection depend on a good mechanism of interpolation because they not only rely on the integration of the trajectories of fluid particles traveling in space but also on the evaluation of quantities at determined points that do not necessarily match to the mesh points. The subject of this paper is to discuss and to survey new capabilities of a high-order interpolation operator using cubic shape functions as well as to demonstrate the reduction of errors originating from a Z-Type approach by considering directional derivatives over every element. This capability translates into a good fit for the convective term embedded into the incompressible Navier-Stokes equations, since the velocity at the departure point, whether it has to be interpolated, is found with more accuracy. Maximum error value obtained is limited to* $\mathcal{O}(10^{-3})$*. A fairly good approximation is produced showing the influence of the directional derivatives calculated over the edges of the element.*

Keywords: *Semi-Lagrangian, Finite Element, Interpolation.*

1. INTRODUCTION

Discrete models using Semi-Lagrangian advection depend on a good mechanism of interpolation because they not only rely on the integration of the trajectories of fluid particles traveling in space but also on the evaluation of quantities at determined points that do not necessarily match to the mesh points. When evoking finite element spaces to generate the discretization process, it is common for some cases to have the mesh points arranged so that they belong to a set of values named *degrees of freedom set*, though this set may not be entirely made up only by the mesh points. This set depends on the geometry of the finite element, the dimension n of a domain lying in the $\mathbb{R}^n$ space and certain requirements that are related to a perfect structuration of function spaces that will be working over each element.

When an application requires more accuracy, it is necessary to think about how to reduce errors. As we have mentioned, Semi-Lagrangian methods are involved with particle trajectories and interpolation. The subject of this paper is to discuss the second item and to survey new capabilities of a high-order interpolation operator using cubic shape functions as well as to demonstrate the reduction of errors due to the interpolation. Zienkiewicz-Type (or Z-Type, in short) interpolation has been developed and experienced in incompressible fluid flow numerical simulations in the work by Oliveira *et al.* (2011).

Hereafter we introduce some basilar concepts for our discussion. Setting the framework to the three-dimensional space, i.e., $n = 3$, we say that $\mathcal{T}^h$ is a *tetrahedralization* of a domain $\Omega \subset \mathbb{R}^3$. It is convenient to define a finite element as a triple (K, P_π, Σ), where K is a tetrahedron, P_π a set of polynomial or quasi-polynomial functions with degree $\leq \pi$ and Σ as the set of degrees of freedom. Moreover, we require that $\Omega = \cup_{m=1}^{M} K_m$, with $\mathring{K}_c \cap \mathring{K}_d = \emptyset \ \forall c, d$. Thus, $\mathcal{T}^h$ is composed of a family of tetrahedra. We denote by $\boldsymbol{a}_j = (x_{1j}, x_{2j}, x_{3j}), 1 \leq j \leq 4$ each vertex of a tetrahedron, so that the first index stands for *direction* and the second one for *number of vertex*. Henceforward, index i will be associated to space directions.

Paper is organized as follows: in the Section 2. we introduce the concepts of affine mappings in finite elements and establish how to prepare the study of Z-Type interpolant; in the Section 3. we lay down and discuss the Z-Type interpolant, its shape functions and how it works; Section 4. shows us some results of interpolation and error analysis; ultimately, we make concluding remarks in the Section 5.

2. UNIT 3-SIMPLEX AND FINITE ELEMENT AFFINE MAPPINGS

Let (K, P, Σ) and $(\hat{K}, \hat{P}, \hat{\Sigma})$ be finite elements defined over the spacial domain and over a reference domain, respectively. K can be mapped to the tetrahedron $\hat{K}$ which is the unit 3-simplex, i.e., a regular tetrahedron whose edges sizes are unitary. The vertices coordinates of $\hat{K}$ are given by: $\hat{\boldsymbol{a}}_1 = (1,0,0)$, $\hat{\boldsymbol{a}}_2 = (0,1,0)$, $\hat{\boldsymbol{a}}_3 = (0,0,1)$ and $\hat{\boldsymbol{a}}_4 = (0,0,0)$. Through an affine mapping, such as $F := K \to \hat{K}$, we get $\hat{\boldsymbol{x}} = F(\boldsymbol{x}) = \boldsymbol{B}(\boldsymbol{x})$, with $\hat{\boldsymbol{x}} \in \hat{K}, \boldsymbol{x} \in K$. F is a mapping defined by $\boldsymbol{B}$, which is a square matrix that maps each point of K to a unique point in $\hat{K}$.

Consider $\boldsymbol{v} = (v_1, v_2, v_3)$ defined over K the velocity field of the fluid flow, where each of v_1, v_2 and v_3 are real-valued functions depending on the space and time, such that $\hat{\boldsymbol{v}} = (\hat{v}_1, \hat{v}_2, \hat{v}_3)$ be equivalent over $\hat{K}$ to $\boldsymbol{v}$. Similarly, let ∇ and $\hat{\nabla}$ be gradient operators defined over these domains, respectively. Now, it is important to define Σ in order to carry out the interpolation over the reference domain. This operation is common in finite elements computations and some reasons are given in Ciarlet (2002) (the most important for us would be that related to the theory of interpolation). Thereby, we define $\Sigma := \{\boldsymbol{v}(\boldsymbol{a}_j), \nabla\boldsymbol{v}(\boldsymbol{a}_j) \cdot (\boldsymbol{a}_k - \boldsymbol{a}_j);\ 1 \leq j \neq k \leq 4\}$. Consequently, not only the values of function, but also the values of directional derivatives over the edges of each tetrahedron are required to develop our survey. It becomes possible to take the values from Σ to $\hat{\Sigma}$ through a mapping, so that $\hat{\Sigma}$ turns into the set of degrees of freedom of the reference finite element. Therefore, $\hat{\Sigma} := \{\hat{\boldsymbol{v}}(\hat{\boldsymbol{a}}_j), \hat{\nabla}\hat{\boldsymbol{v}}(\hat{\boldsymbol{a}}_j) \cdot (\hat{\boldsymbol{a}}_k - \hat{\boldsymbol{a}}_j);\ 1 \leq j \neq k \leq 4\}$ and we have

$$\{\nabla\left[\boldsymbol{v}(\boldsymbol{a}_j)\right]\} \cdot (\boldsymbol{a}_k - \boldsymbol{a}_j) = \{\hat{\nabla}\left[(\hat{\boldsymbol{v}} \circ \boldsymbol{B})(\boldsymbol{a}_j)\right]\} \cdot (\boldsymbol{a}_k - \boldsymbol{a}_j) = \{\hat{\nabla}\left[\hat{\boldsymbol{v}}(\boldsymbol{B}(\boldsymbol{a}_j))\right] \hat{\nabla}\left[\boldsymbol{B}(\boldsymbol{a}_j)\right]\} \cdot (\boldsymbol{a}_k - \boldsymbol{a}_j), \tag{1}$$

whence it follows that $\nabla\left[\boldsymbol{B}(\boldsymbol{a}_j)\right]$ is a second order tensor representing the *Jacobian*, once that the operators $\nabla = \left(\frac{\partial}{\partial x_1}, \frac{\partial}{\partial x_2}, \frac{\partial}{\partial x_3}\right)$ and $\hat{\nabla} = \left(\frac{\partial}{\partial \hat{x}_1}, \frac{\partial}{\partial \hat{x}_2}, \frac{\partial}{\partial \hat{x}_3}\right)$ lie in different frames and operate over a vector. "$\circ$" is a symbol for a "pseudo-composition" of functions, since we use derivation as the chain rule. We should note that from Eq. (1) the derivatives belonging to Σ also are mapped to $\hat{\Sigma}$ in order to complete the degrees of freedom required for the Z-Type interpolation operator to be discussed in the Sec. 3.

If we name $\boldsymbol{\xi}_{jk} = \boldsymbol{a}_k - \boldsymbol{a}_j$, and segregate $\nabla\boldsymbol{v}$ in the parcels $\nabla_1\boldsymbol{v} = \left(\frac{\partial v_1}{\partial x_i}\right)$, $\nabla_2\boldsymbol{v} = \left(\frac{\partial v_2}{\partial x_i}\right)$ and $\nabla_3\boldsymbol{v} = \left(\frac{\partial v_3}{\partial x_i}\right)$, which are the contributions of variations of the velocity for each direction, then the directional derivatives over the edges of a tetrahedron on the spacial frame can be given by:

$$\nabla_i\boldsymbol{v} \cdot \boldsymbol{\xi}_{jk} = \frac{\partial \boldsymbol{v}}{\partial \boldsymbol{\xi}_{jk}}, \tag{2}$$

Throwing in ϕ as a scalar field defined over $\mathbb{R}^3$, it is clear that $\nabla\phi$ is a vector with three components, which we depict geometrically in the Fig. 1. We see how the directional derivatives are decomposed over the edges of a tetrahedron in space through $\nabla\phi$, whose origin is the vertex a_j and A it is a point lying in the straight line of variation. A_1, A_2 and A_3 are points belonging to each adjacent edge to a_j and working in the sense of the Eq. (2), like the projections of $\nabla\phi$. In fact, these points represent the directional derivatives. The punctured points identify the value in norm of the gradient at each vertex. The decomposition of $\nabla\phi$ in K is homologous in $\hat{K}$ as it is pictured in Fig. 2. However, the value of the projections differ from that over K because of the measure of the edges. Equation (1) tells us that $\nabla\boldsymbol{B}$, i.e., the tensor associated to the Jacobian transformation, is responsible to carry over the behavior of the variations of the function from K to $\hat{K}$. In this example, $n = 1$, but the same idea can be extended to $n \geq 2$.

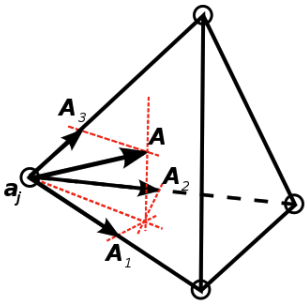

Figure 1: Directional derivatives of a scalar ϕ over the edges of a tetrahedron in the space.

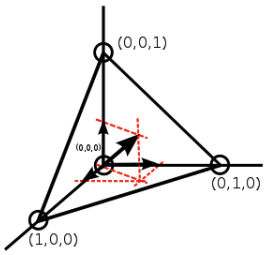

Figure 2: Directional derivatives of a scalar ϕ over the edges of the unit 3-simplex.

3. DISCUSSION ABOUT THE FE Z-TYPE INTERPOLATION OPERATOR

The interpolation operator is denoted by $\mathcal{I}_3$. Due to the change of frame (see Eq. (1)), a not very discernible result at first glance, holds, which is declared as

$$\widehat{(\mathcal{I}_3 \boldsymbol{v})} = \hat{\mathcal{I}}_3 \hat{\boldsymbol{v}}, \tag{3}$$

claiming that what we get after carrying out the interpolation over K and take it away to $\hat{K}$ through the change of referential is the equivalent result of carrying out an interpolation over $\hat{K}$, since that mathematically another interpolation operator defined over $\hat{K}$ should operate over $\hat{\boldsymbol{v}}$.

By invoking the linear functions $\lambda(\hat{\boldsymbol{x}}), 0 \leq \lambda(\hat{\boldsymbol{x}}) \leq 1$, which also are the barycentric coordinates over $\hat{K}$, we reach

$$\hat{\mathcal{I}}_3 \hat{\boldsymbol{v}}(\hat{\boldsymbol{x}}) = \sum_{l=1}^{4} \hat{\boldsymbol{v}}(\hat{\boldsymbol{x}}_l)\lambda_l(\hat{\boldsymbol{x}}) + \sum_{j=1}^{4}\sum_{k=1}^{4} \left[\hat{\nabla}\hat{\boldsymbol{v}}(\hat{\boldsymbol{a}}_j) \cdot (\hat{\boldsymbol{a}}_k - \hat{\boldsymbol{a}}_j) - \sum_{l=1}^{4} (\hat{\boldsymbol{v}}(\hat{\boldsymbol{a}}_l)\hat{\nabla}\lambda_l(\hat{\boldsymbol{x}})) \cdot (\hat{\boldsymbol{a}}_k - \hat{\boldsymbol{a}}_j) \right] \lambda_{jk}(\hat{\boldsymbol{x}}), \tag{4}$$

where

$$\lambda_{jk}(\hat{\boldsymbol{x}}) = \frac{1}{2}\left[\lambda_j(\hat{\boldsymbol{x}})\lambda_k(\hat{\boldsymbol{x}}) + \lambda_j^2(\hat{\boldsymbol{x}})\lambda_k(\hat{\boldsymbol{x}}) - \lambda_j(\hat{\boldsymbol{x}})\lambda_k^2(\hat{\boldsymbol{x}})\right], \quad 1 \leq j,k \leq 4, \tag{5}$$

are a parcel of the shape functions of TE16 element established in Wang and Xu (2006) and $\hat{\nabla}_l(\hat{\boldsymbol{x}})$ are the gradients of the barycentric coordinates. Implicitly, the inner products are being reckoned through the space directions.

We have seen in Sec. 2.that the elements $K \in \mathcal{T}^h$ are mapped to $\hat{K}$ by an affine transformation. It was argued how this change of frame just conveys the information of a function to a simpler domain without removing the interpolation capability. Now, we turn to a survey by considering translations and rotations. Besides, we discuss how this latter process still remains preserved, i.e., we show that the interpolation is well conserved under translation and rotation.

In order to pave the way to the numerical results, we render two operators for the geometric changes. Firstly, a translation will be given by a simple displacement of the points of $\hat{K}$, i.e., by fixing a vector $\boldsymbol{d} = (d_1, d_2, d_3)$ and defining

$\hat{K}_{\boldsymbol{d}} := \hat{K} + \boldsymbol{d}$ as the whole $\hat{K}$ displaced in space. Either, it would be read as

$$\hat{K}_{\boldsymbol{d}} := \{\boldsymbol{y} \in \mathbb{R}^3;\, \boldsymbol{y} = \hat{\boldsymbol{x}} + \boldsymbol{d}\}. \tag{6}$$

In second place, a rotation matrix gathering the Euler's proper angles, which are a triple (ψ, θ, φ), for $0 \leq \theta \leq \pi$ and $0 \leq \psi, \varphi \leq 2\pi$, relating two systems of coordinates. Here, we will use a simple rotation matrix. More specific studies can be found in the treatise on rotational motion by Gray (1918). We define that rotation matrix by

$$R(\psi,\theta,\varphi) = \begin{bmatrix} cos(\theta)\,cos(\varphi) & -cos(\varphi)\,sin(\psi) + sin(\varphi)\,sin(\theta)\,cos(\psi) & sin(\varphi)\,sin(\psi) + cos(\varphi)\,sin(\theta)\,cos(\psi) \\ cos(\theta)\,sin(\psi) & cos(\theta)\,cos(\psi) + sin(\varphi)\,sin(\theta)\,sin(\psi) & -sin(\varphi)\,cos(\psi) + cos(\varphi)\,sin(\theta)\,sin(\varphi) \\ -sin(\theta) & sin(\varphi)\,cos(\theta) & cos(\theta)\,cos(\varphi) \end{bmatrix}, \tag{7}$$

whose operation is to carry out a composition of partial rotations on the points of $\hat{K}$. It suffices accompany this effect by observing a certain "invariance" of the interpolation at the interior points, as we will see forth. Thus, through (6) and (7), a huge range of numerical experiments can be done to test out the interpolation.

4. NUMERICAL RESULTS

Some results are introduced in this section by considering the interpolation of the vector field $\hat{\boldsymbol{v}}$ over $\hat{K}$ on a tridimensional grid with 9261 nodes. Since each component of $\hat{\boldsymbol{v}}$ is interpolated in a similar fashion, it is enough survey the results given by only one of them.

The series of figures forward opens up the numerical results we have implemented. A cubic polynomial is being

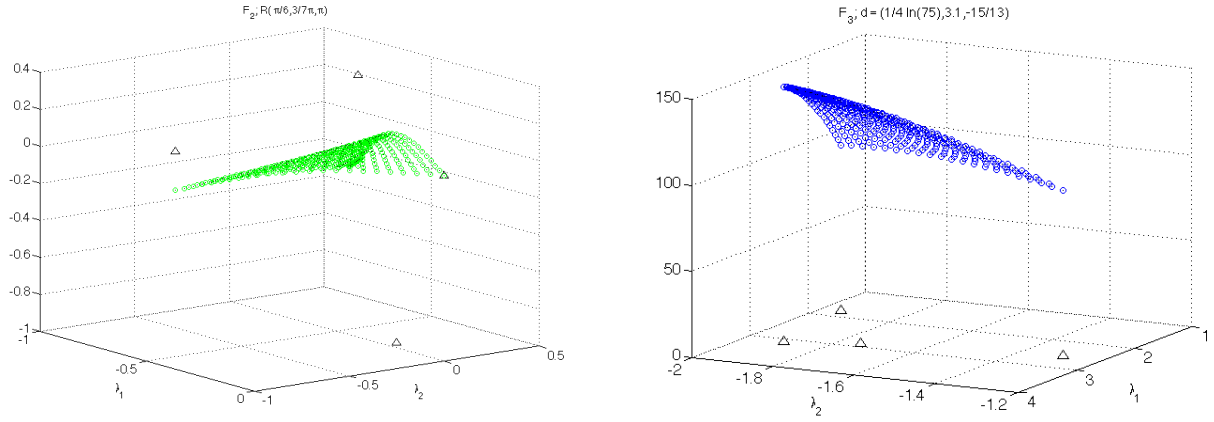

(a) (b)

Figure 3: (a) depicts a rotation of $\hat{F}_2$ by $R(\pi/6, 3\pi/7, \pi)$; (b) depicts a translation of $\hat{F}_3$ by $\boldsymbol{d} = (1/4\,ln(75), 3.1, -15/13)$.

interpolated over the unit 3-simplex domain. The small points in black encircled by colors are the fitted points forming the interpolation. Colors are representing the function value restricted to each face of the unit 3-simplex, namely, red to face 1, green to face 2, blue to face 3 and magenta to face 4. Figure 3 shows two plots of function just restricted to the faces 2 and 3 of $\hat{K}$. These faces are defined as $\hat{F}_2$ and $\hat{F}_3$, respectively, because they are opposed to the correspondent vertices $\hat{\boldsymbol{a}}_2$ and $\hat{\boldsymbol{a}}_3$. Similarly, the two remaining faces obey this relation. Because of the continuity and the affine mapping, the values of $\hat{\boldsymbol{v}}$ over the edges of $\hat{K}$ are such as:

$$\hat{\boldsymbol{v}}|_{\hat{F}_{mn}} := \hat{\boldsymbol{v}}|_{\hat{F}_m} \cap \hat{\boldsymbol{v}}|_{\hat{F}_n}, \quad m \neq n. \tag{8}$$

The four triangles (when they appear) spreaded over the plots pin the original points of each vertex before suffering

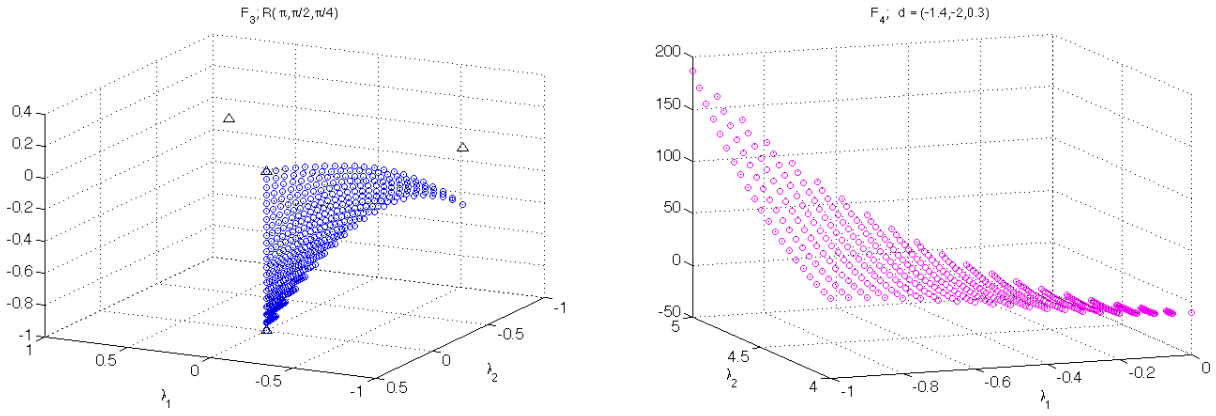

(a) (b)

Figure 4: (a) depicts a rotation of $\hat{F}_3$ by $R(\pi, \pi/2, \pi/4)$; (b) depicts a translation of $\hat{F}_4$ by $\boldsymbol{d} = (-1.4, -2, 0.3)$.

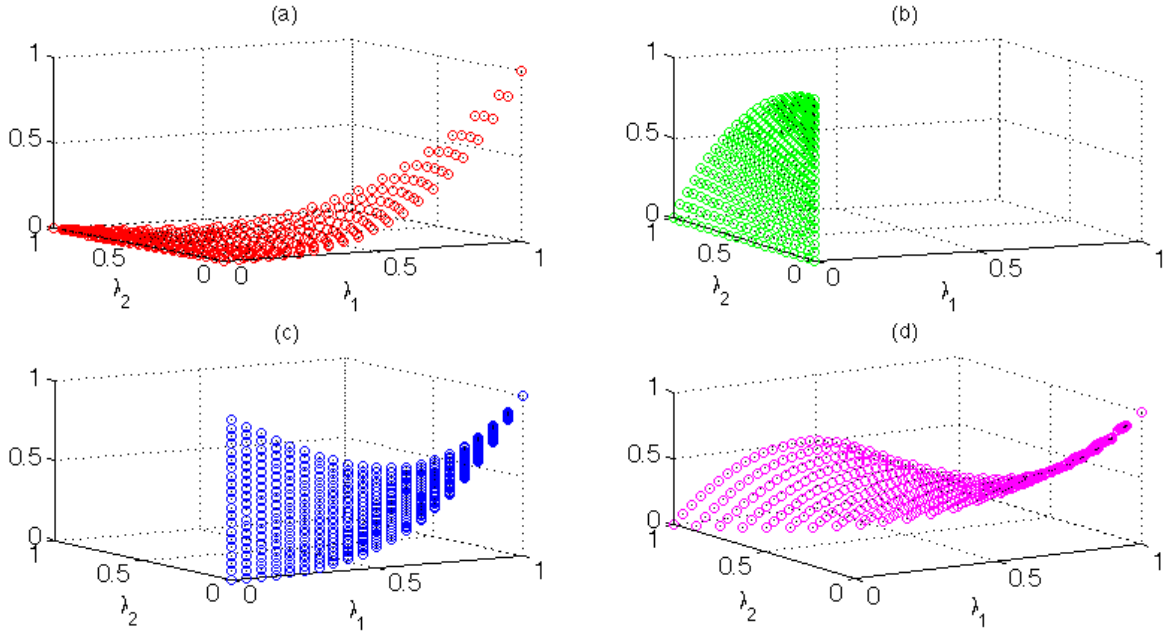

Figure 5: (a), (b), (c) and (d) depict $\hat{\boldsymbol{v}}|_{\hat{F}_1}, \hat{\boldsymbol{v}}|_{\hat{F}_2}, \hat{\boldsymbol{v}}|_{\hat{F}_3}$ and $\hat{\boldsymbol{v}}|_{\hat{F}_4}$ for the cubic case, respectively.

any transformation. In Fig. 3, at left we have a simple rotation of $\hat{F}_2$ by $R(\pi/6, 3\pi/7, \pi)$, whereas at right we have a simple translation of $\hat{F}_3$ by $\boldsymbol{d} = (1/4\, ln(75), 3.1, -15/13)$. These transformations do not harm the interpolation, which is ensured by Eq. (3).

Other examples of transformations are depicted in Fig. 4. Now, $\hat{F}_3$ is rotated by $R(\pi, \pi/2, \pi/4)$ and, additionally, $\hat{F}_4$ is translated by $\boldsymbol{d} = (-1.4, -2, 0.3)$. As we had already commented, uncountable and arbitrary transformations can be set by changing the parameters for angles and displacement. Forth, Fig. 5 gathers the plots of function over all faces originally (i.e. without suffering transformations) by exhibiting them apart, accordingly to (8).

In order to enrich our survey, we also plot below some examples of interpolation when $\boldsymbol{v}$ is reduced to a quadratic curve or to a plane. Figure 6 shows the same as Fig. 5 for the quadratic case. In turn, Fig. 7 shows the plots for the linear case. For both two latter cases, we could apply the same tests already performed, by concluding that the interpolation would not be harmed.

All the results from the mechanism of interpolation exhibit an utmost capability for the treatment of the convective term embedded into the incompressible Navier-Stokes equations, since the velocity at the departure point, whether it has

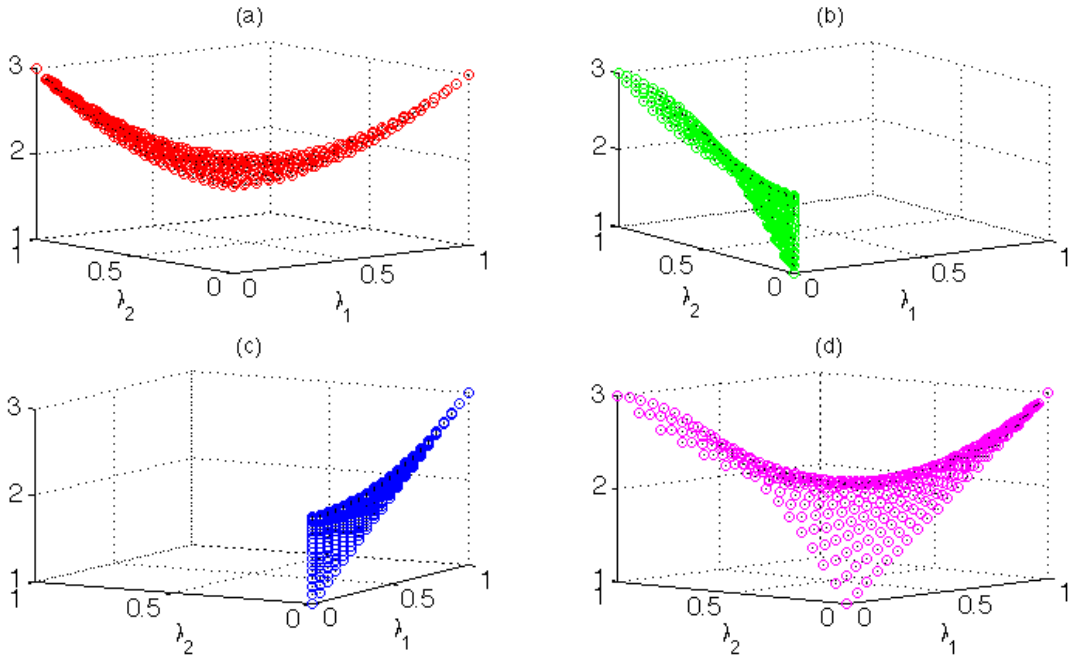

Figure 6: (a), (b), (c) and (d) depict $\hat{\boldsymbol{v}}|_{\hat{F}_1}$, $\hat{\boldsymbol{v}}|_{\hat{F}_2}$, $\hat{\boldsymbol{v}}|_{\hat{F}_3}$ and $\hat{\boldsymbol{v}}|_{\hat{F}_4}$ for the quadratic case, respectively.

to be interpolated, is found with more accuracy.

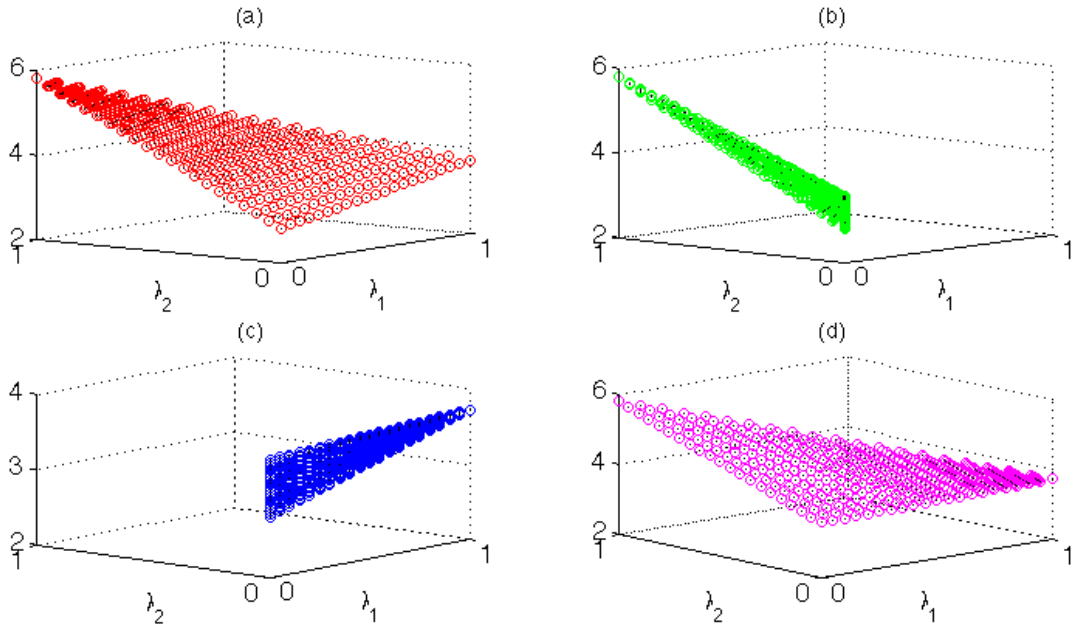

Figure 7: (a), (b), (c) and (d) depict $\hat{\boldsymbol{v}}|_{\hat{F}_1}$, $\hat{\boldsymbol{v}}|_{\hat{F}_2}$, $\hat{\boldsymbol{v}}|_{\hat{F}_3}$ and $\hat{\boldsymbol{v}}|_{\hat{F}_4}$ for the linear case, respectively.

Finally, an brief discussion about the error of interpolation is given. $\mathcal{L}_2$-norm error between $\hat{\boldsymbol{v}}$ and $\hat{\mathcal{I}}_3\hat{\boldsymbol{v}}$ is plotted in Fig. 8 for $\hat{F}_1$. It is seen that the minimum error is checked at the boundary, whereas it enhances as it goes towards the center. However, the maximum error value is limited to $\mathcal{O}(10^{-3})$, according to a purpose we have been aspiring. We can observe that along the edges of $\hat{F}_3$, the approximation is well done and this result reasonably verifies the influence of the directional derivatives calculated over them which extends to the interior of $\hat{K}$. Clearly, some deviation of $\hat{\mathcal{I}}_3\hat{\boldsymbol{v}}$ from $\hat{\boldsymbol{v}}$ is more sharply observed in the middle of the face, where there is presence of a more acute curvature of $\hat{\boldsymbol{v}}$. Figure 9 is a

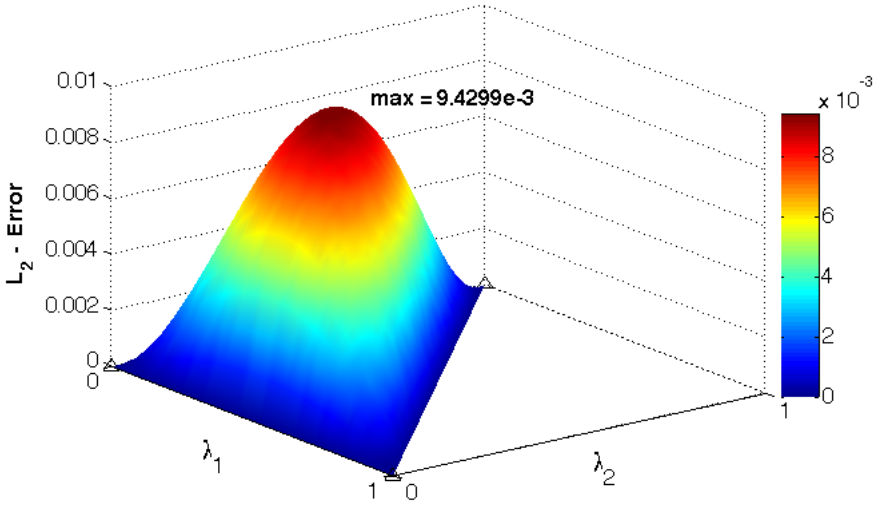

Figure 8: $\mathcal{L}_2$-norm error between $\hat{\boldsymbol{v}}$ and $\hat{\mathcal{I}}_3\hat{\boldsymbol{v}}$.

complementary error contour with $\hat{\boldsymbol{v}}$ scaled exaggeratedly over the domain.

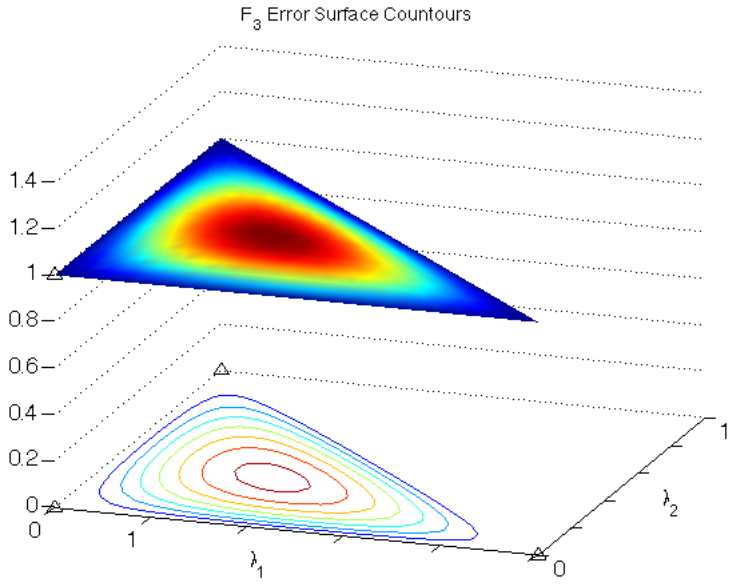

Figure 9: Error contour of $\hat{\mathcal{I}}_3\hat{\boldsymbol{v}}$ over $\hat{F}_1$.

5. CONCLUSION AND FUTURE PROSPECTS

The main purpose of our essay was to weave a mechanism of interpolation for Semi-Lagrangian schemes in order to get more accuracy in fluid flow simulations through the Finite Element Method. The results we previously analyzed showed that error diminished over the element of reference. However, the greatest deviation occurring nearby the center of $\hat{K}$ may be related to an incomplete polynomial basis, since we have used 16 degrees of freedom for each component of $\boldsymbol{v}$. For cubic approximations, the presence of some additional degrees of freedom, such as those that are included at the midpoints of the faces, may afford more accurate results inasmuch as they could gauge the deviation at that central regions.

Rotation and translation tests were a way to launch an expectation that the interpolation works suitably even than the

element suffers these geometric changes and also attends to accuracy requirements for fluid flow numerical simulations. When keeping this capability to capture the behavior of a cubic function, the interpolation just reinforces its own validity for the intended applications.

Future prospects for this research are: to apply this Z-Type interpolation methodology in more complex simulations; to develop comparative methods including derivative calculations and to study improvements by integrating this approach into a more robust computational code.

6. REFERENCES

Ciarlet, P., 2002. *The Finite Element Method for Elliptic Problems*. SIAM, New York, United States.

Gray, A., 1918. *A Treatise on Gyrostatics and Rotational Motion*. MacMillan and Co., London, England.

Oliveira, G., Mangiavacchi, N. *et al.*, 2011. "A semi-lagrangian scheme for fluid flow simulations with a zienkiewicz-type finite element interpolation". In *21st International Congress of Mechanical Engineering*.

Wang, M. and Xu, J., 2006. "Some tetrahedron nonconforming elements for fourth order elliptic equations". In *Report AM290 from PennState University*.

7. RESPONSIBILITY NOTICE

The authors are the only responsible for the printed material included in this paper.